EXPERIMENTAL AND NUMERICAL SIMULATION STUDY OF SODIUM HEAT PIPE WITH LARGE ASPECT RATIO

by

Shuaijie SHA, Huikang CAI, Hanzhong TAO, Yannan LI*, Chao SONG, and Junjie WANG

School of Energy Science and Engineering, Nanjing Tech University, Jiangsu, China

Original scientific paper
https://doi.org/10.2298/TSCI231030059S

As a core cooling device of reactor, a high temperature sodium heat pipe is designed in this paper which has a large aspect ratio of 126. The effects of heating mode and evaporation section length on its start-up are studied experimentally. The results show that the axial temperature uniformity of the heat pipe is better under variable power heating mode. As the evaporation cross-section length increases, thermal resistance decreases by 50%. Compared with heat pipes with low aspect ratio, heat pipes with large aspect ratio are more difficult to start up. Furthermore, numerical simulation is conducted on the designed sodium heat pipe to acquire the velocity and pressure distribution during steady-state operation.

Key words: *large aspect ratio, startup characteristics, sodium heat pipe*

Introduction

Heat pipe-encapsulated nuclear heat source (HP-ENHS) reactor is designed by using the elements in the core concept of SAFE-400 space reactor [1], which is different from the original encapsulated nuclear heat source (ENHS) reactor [2]. The reactor utilizes an alkali metal heat pipe (HP) to extract heat from the solid core, offering several advantages such as enhanced passive decay heat removal capacity, absence of a positive void coefficient, and relatively low cladding corrosion [3]. At present, due to the close relationship between the HP and core heat transfer, the research of HP has become a hot spot in HP-ENHS reactor. As an efficient energy-saving heat transfer device, HP can convey a substantial amount of heat over long distances through the working medium in the pipe-line without requiring an external power source [4]. For nuclear reactors operating at temperatures exceeding 500 °C, alkali metals such as sodium, potassium, lithium, *etc.*, are commonly employed as the working medium in HP.

The startup characteristic of the HP is one of the keys to analyzing and estimating the performance of HP. A successful start-up is a prerequisite for HP operation [5]. Therefore, researchers have carried out a series of studies on the startup of alkali metal HP. Among them, the effect of heating power is studied. Zhang *et al.* [6] performed an experimental investigation on a 1 m long, 25 mm diameter sodium-potassium alloy HP under forced convection cooling. They also explored the geyser boiling phenomenon of the sodium-potassium alloy during start-up under varying input power. The study revealed that the HP achieves a quicker start-up time under geyser boiling conditions. Jang [7] carried out experimental research on potassium HP heated by different input power in the vacuum chamber. It was found that the HP can be started

* Corresponding author, e-mail: liyannan@njtech.edu.cn

quickly under the condition of high input power. Chen *et al.* [8] experimentally explored the starting characteristics of a cesium HP with an aspect ratio of 19 in a horizontal state. The start-up temperature curves of the HP heated by different input power were compared. On the basis of the dusty gas model, Tournier *et al.* [9] established a free molecule, transition and continuous steam flow model, and analyzed the performance of a sodium HP under the condition of radiation cooling. Ge *et al.* [10] developed an unsteady analysis program for high temperature HP to simulate the complex phase transitions, steam flow and mass and heat transfer characteristics at the gas-liquid interface involved in the start-up process of sodium HP self-solidification state, and verified the accuracy of the program through experimental data.

In addition, the tilt angle is also a contributing factor influencing the startup of the HP. Ma *et al*. [11] experimentally explored the sodium HP with an aspect ratio of 38 in the range of –15° to 45° and analyzed the freezing startup characteristics of the sodium HP when placed near horizontally. Wang *et al*. [12] carried out experimental research on high temperature potassium HP with an aspect ratio of 27 in the range of –15° to 90°. The results certified that the tilt angle could significantly shorten the startup time and minimum input power of the HP within 15°. Yang *et al*. [13] developed a surface plate sodium HP receiver and tested it in the range of 30° to 90°. The results showed that when the tilt angle varied from 45° to 90°, the freezing startup time of the HP increased. Yu *et al*. [14] conducted an experimental study on the high temperature sodium HP with combined cores and triangular grooved cores and analyzed the influence of cooling on these two HP under different inclinations. Guo *et al*. [15] studied the startup characteristics of a sodium-potassium alloy HP with a pipe length of 1000 mm and pipe diameter of 25 mm in the range of 0° to 50°. The findings indicated that with an increase in the tilt angle, the startup performance of the HP improved. At 0°, 30°, and 90° inclination angles, Ding *et al.* [16] experimentally studied a high temperature HP with a specific size. Yu *et al.* [17] analyzed the internal flow field characteristics of sodium HP at different angles based on CFD method. The results show that the pressure drop in the gas phase is essentially unaffected by the working condition of the tilt angle. The gas-liquid-flow velocity is almost independent of the inclination angle.

Although previous researchers have done a lot of research on the startup characteristics of high temperature sodium heat pipe (HTSHP), the ratio of length to diameter of sodium heat pipe (SHP) studied in the past is far less than 100. The larger the length-diameter ratio, the greater the driving force required for the circulating flow of working fluid in the pipe, and the more difficult the start-up of the HP. Hence, this paper presents the design of a SHP with a length-to-diameter ratio of 126. Subsequently, experimental investigations are conducted to examine its startup characteristics. Furthermore, the diphasic flow of the working medium in the SHP is simulated using FLUENT software. This simulation allows for the evaluation of crucial thermal parameters, including the flow rate and pressure drop in the steam chamber and the suction core within the heat pipe.

Experimental device

Experimental equipment

The specific parameters of the HP geometry are listed in tab. 1. It is made of stainless steel and filled with 130 g of Na. Sodium has a higher boiling point and heat conductance than other alkali metals (such as potassium and sodium-potassium alloys), which makes metal sodium have a wider operating margin and higher heat transfer capacity. Therefore, we choose sodium as the working medium to fill the HP. A core structure composed of two layers of tungsten wire mesh is installed in the SHP. The SHP is filled by the method introduced in the [18]. The sodium is initially operated on in the glove box and protected by inert gases. Then, the SHP is vacuumed to 10^{-6} Pa by a high vacuum pump device and filled with sodium. The SHP needs to be kept at a high temperature throughout the filling process to ensure that the sodium does not condense into a solid during the injection process.

Owing to the large surface tension of liquid metal sodium, a composite screen wick is arranged inside the SHP. This is because the screen wick has the characteristics of good performance, low cost, and convenient manufacture, and the composite wick can provide large circulating capillary force and reflux permeability for the fluid.

Table 1. Parameters of SHP

Parameter	Specifications
Outer diameter of SHP, D_0	19 mm
Thickness of SHP, δ	1.5 mm
Length of SHP, L	2400 mm
Filling quantity	130 g
Mesh number of wick	50 mesh + 400 mesh
Tube material	stainless steel

As shown in fig. 1, an experimental device is built to test the startup characteristics of the SHP. The heating furnace and SHP are fixed on the test bench. There are angle-adjusting devices on both sides of the test bed to adjust the inclination angle of the SHP. According to the geometry of the SHP and the length of the heating furnace, the evaporation section (ES) and condensation section (CS) of the SHP are set to 1200 mm and 1200 mm, respectively. The input heat of the ES is provided by the heating iron wire in the heating furnace. Under the control of the contact voltage regulator, the maximum heat that can be provided is 12 kW. A temperature sensor is installed in the furnace to monitor the temperature in the furnace in real-time. The furnace diameter is slightly larger than the outer diameter of the heat pipe so that the heat pipe can

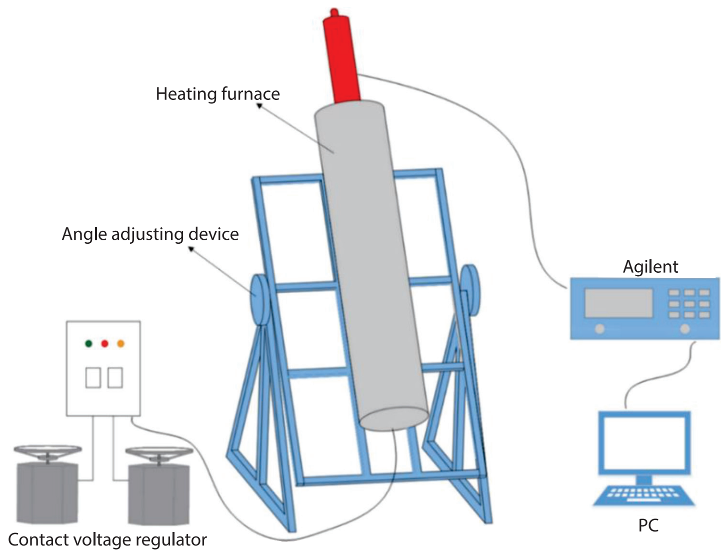

Figure 1. Schematic diagram of experimental system

insert into the furnace smoothly. As shown in figs. 2 and 13 thermocouples with an accuracy of ±1.5 °C are set on the outer wall of the SHP to measure the wall temperature of the ES and the CS. Among them, T_1-T_7 are arranged in the ES and T_8-T_{13} are arranged in the CS. The temperature changes of all measuring points are recorded by the Agilent data acquisition instrument (34970 A), with a period of 1.5 seconds. There is a 10 mm thick insulation layer in the heating furnace to avoid heat loss inside the furnace.

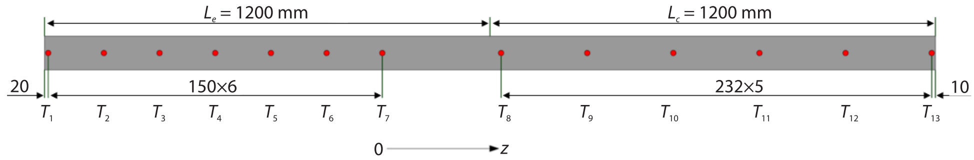

Figure 2. Thermocouple position in axial direction of SHP

Experimental procedures

First, the SHP was tested under two diverse heating modes. One mode is at fixed power Q_7 heating. The other mode is heating with variable power (the heating power is adjusted from Q_1-Q_7, and the adjustment period is 25 min). The values of heating power during the experiment are shown in tab. 2. Then, the temperature changes during the startup of the SHP under different ES lengths are compared. The specific test conditions are shown in tab. 3. Considering a range of factors such as laboratory conditions and the relative difficulty of starting the SHP, in this paper we only studied the impact of varying the length of the two ES. The working temperature of the SHP during all experiments is 650 °C.

Table 2. Calibration values of heating powers

	Q_1	Q_2	Q_3	Q_4	Q_5	Q_6	Q_7
Heating power [W]	153.7	393.4	743.7	1204.7	1776.3	2458.5	3251.4

Table 3. Test conditions

Experiment number	Length of ES	Length of CS
1	1200 mm	1200 mm
2	1225 mm	1175 mm

Data processing and error analysis

The thermal characteristics of SHP during start-up are studied by tube wall temperature and equivalent thermal resistance. The equivalent thermal resistance:

$$R_{\text{sys}} = \frac{T_\text{e} - T_\text{c}}{Q_\text{in}} \tag{1}$$

Based on the physical properties of the alkali metal inside the high temperature HP, the startup procedure of the alkali metal HP is divided into three-stages: free molecular flow (Kn > 1), transition flow (0.01 < Kn < 1) and continuum flow (Kn < 0.01), which are expressed by dimensionless Knudsen number:

$$\text{Kn} = \frac{\lambda}{D_\text{v}} \tag{2}$$

where

$$\lambda = \frac{1.05\kappa T}{\sqrt{2}\pi\sigma^2 P}$$

and the Boltzmann constant κ is taken as $1.38\cdot10^{-23}$ J/K and effective molecular diameter of sodium σ is $3.58\cdot10^{-10}$ m.

When steam changes from free molecular flow to transition flow and then to continuous flow, each flow state transition corresponds to a transition temperature. The gas transition temperature can be calculated [19]:

$$T_{\mathrm{tr}} = \frac{\sqrt{2}\pi\sigma^2 \mathrm{Kn} D_{\mathrm{v}} P_{\mathrm{sat}}}{1.05\kappa} \tag{3}$$

where P_{sat} is the vapor saturation pressure corresponding to T_{tr}, which can be obtained [20]:

$$\lg P_{\mathrm{sat}} = 11.36 - \frac{5567}{T_{\mathrm{tr}}} - 0.50\lg T_{\mathrm{tr}} \tag{4}$$

Through the iterative calculation of eqs. (3) and (4), the transition temperature of sodium vapor from free molecular flow to transition flow in this experiment is 281 °C. The transition temperature from transition flow to continuous flow is 433 °C.

Uncertainty is an index to measure the quality of measurement results, which reflects the reliability of the results. In this paper, the uncertainty of experimental data is calculated by using the law of error propagation. For example, the uncertainty of equivalent thermal resistance of heat pipe in this test:

$$\frac{\Delta R_{\mathrm{sys}}}{R_{\mathrm{sys}}} = \sqrt{\left(\frac{\Delta(T_{\mathrm{e}})}{T_{\mathrm{e}}}\right)^2 + \left(\frac{\Delta(T_{\mathrm{c}})}{T_{\mathrm{c}}}\right)^2} \tag{5}$$

Results and discussion

In the experiment, the CS adopts two heat dissipation modes:

– he CS is provided with an insulating cover and
– the CS is exposed to air.

The experimental results show that when the CS is exposed to the air, the cooling speed of the CS is too fast, and the thermal resistance between the CS and the external environment is small so the working medium of the CS is not easy to melt, and the SHP cannot be started smoothly. Therefore, in all the following experiments, the CS of the SHP is dissipated by adding a heat shield.

Description of the frozen startup process

Figure 3 shows the wall temperature variation of the SHP during freezing startup under 3251.4 W input power. As shown in fig. 3, in the first 14 minutes, the wall temperature of the ES is lower than the melting point temperature of metal sodium (97.72 °C). During this period, most of the input heat is used to heat and melt the alkali sodium in the SHP. With the continuous input of heat, a small amount of sodium begins to evaporate and flows in the gas chamber of the ES in the free-molecule state. However, the gas is too sparse and the heat transferred to the CS is very small. Therefore, after 14 minutes, the wall temperature of the ES rises sharply, while the temperature of the CS is almost kept at room temperature.

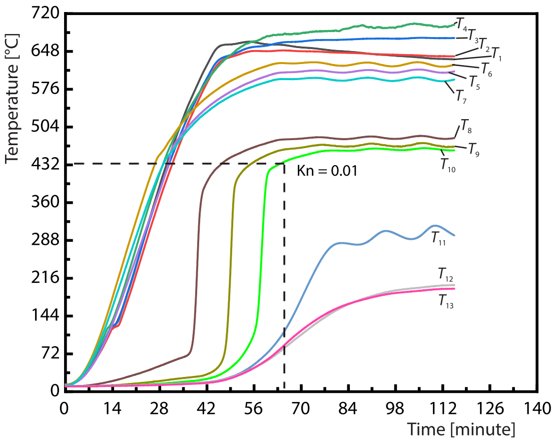

Figure 3. The temperature evolutions of the SHP during freezing start under 3251.4 W heating power

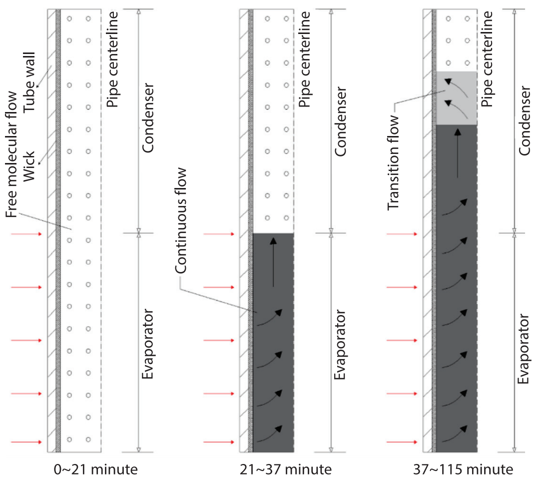

Figure 4. Schematic diagram of the freezing start process

When the heating operation lasts for 28 minutes, the wall temperature of the ES is higher than 433 °C (Kn = 0.01), which indicates that the sodium vapor in the ES of the SHP has been in a continuous flow state. Owing to the elevated density and pressure of the continuous gas-flow, the downward gas temperature gradient (temperature front) at the connection moves to the CS with time and transmits a great deal of heat. Therefore, after 37 minutes, the temperature at measuring points T_8-T_{10} on the CS begins to rise sharply and reaches 433 °C (Kn = 0.01) within 18 minutes. After 115 minutes, the wall temperature of the SHP remains unchanged, indicating that SHP has been running stably. The entire freezing start procedure is shown in fig. 4.

It can also be found from fig. 3 that the temperature at measuring points T_{11}-T_{13}, and on the CS of SHP is obviously lower than 433 °C, which indicates that some sodium steam in the CS of the SHP is not in the continuous flow state. This phenomenon may be caused by the following two reasons:

– Under the heating power of 3251.4 W, the pressure difference in the tube is not enough to push the temperature front to move towards the top of the CS.
– A small amount of non-condensable gas inevitably accumulates near the liquid-gas interface at the top of the CS, forming a non-condensable gas layer, which hinders the condensation heat transfer of steam and boosts the condensation heat transfer resistance [21].

In this paper, when the temperature at the top of the CS is higher than 433 °C, the SHP is considered to have been totally activated. Therefore, under the heating power of 3251.4 W, the SHP did not complete the startup.

Effect of heating mode

Figure 5 illustrates curves depicting the axial temperature variation of the SHP during startup, exhibiting two distinct heating modes. Although the changes in sodium flow state in the two heating modes are similar, there are still some differences in the axial temperature distribution between the two heating modes. As shown in fig. 5, compared with fixed power heating, the axial wall temperature of the ES of the SHP shows better uniformity in the variable power heating mode. This is because the variable power heating mode increases the input power from Q_1-Q_7 every 25 minutes. After being operational for 25 minutes under a certain heating power, the sodium steam flow produced has sufficient time to achieve even distribution within the air cavity of the ES in the SHP.

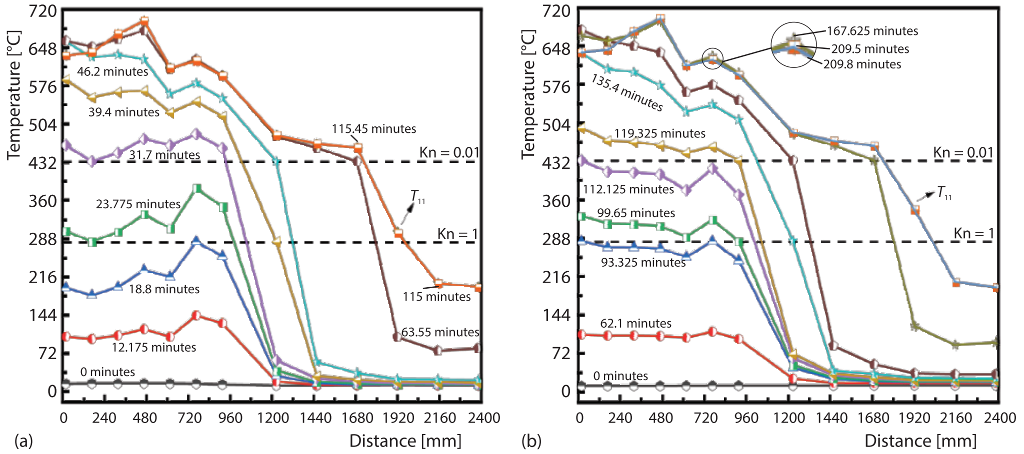

Figure 5. Axial temperature variation of SHP under two heating modes during startup; (a) fixed power (Q_7) and (b) variable power (Q_1-Q_7)

Additionally, in both heating modes, a fraction of the sodium steam located at the upper section of the CS of the SHP does not exhibit continuous flow characteristics. The specific reasons are described in the previous section. The starting time of heating at fixed power is 115.45 minutes, whereas it extends to 209.8 minutes when using variable power. However, the temperature at measuring point T_{11} of the CS of the SHP under the variable power heating mode is higher than that under the fixed power heating mode. This phenomenon can also be seen in fig. 6. Based on fig. 6, it can be observed that during the SHP's stabilization phase, the temperature at measuring point T_{11} on the condensing section is found to be 43 °C higher in the variable power heating mode compared to the fixed power heating mode. Compared to the fixed power heating mode, the variable power heating mode may result in an increased pressure differential within the tube, leading to a displacement of the temperature front towards the upper section. However, it should be noted that there exists a certain amount of non-condensable gas at the top, which consequently causes temperature elevation solely at one specific measuring point. This suggests that variable power heating has the potential to enhance the top temperature of the CS.

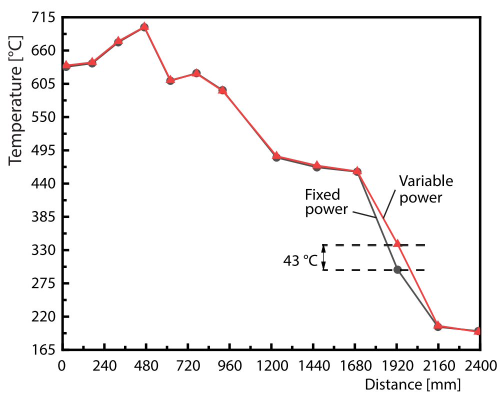

Figure 6. Axial temperature distribution of SHP under two heating modes in steady-state

Effect of ES length

Figure 7 show the evolution of wall temperature during the startup of the SHP when the length of the ES is 1200 mm and 1225 mm, respectively. As observed in fig. 7, when the ES length increases from 1200-1225 mm, the wall temperature of the SHP's ES exhibits a similar change during startup. However, it is noteworthy that the temperature rise rate of the CS's wall, with an ES length of 1225 mm, is significantly faster compared to that with an ES length of 1200 mm. This is because when the length of the ES increases, the filling rate of the working medium in the SHP decreases relatively, resulting in more bubbles generated by phase change in the ES of the SHP when the same power is input, thus driving more heat fluid to move to the CS. Simultaneously, with a decrease in the length of the CS, the cooling rate also decreases, making it easier for the working medium sodium in the CS to melt. Owing to the presence of non-condensable gas, when the ES is 1225 mm long, a small portion of the temperature at the top of the CS remains below 433 °C.

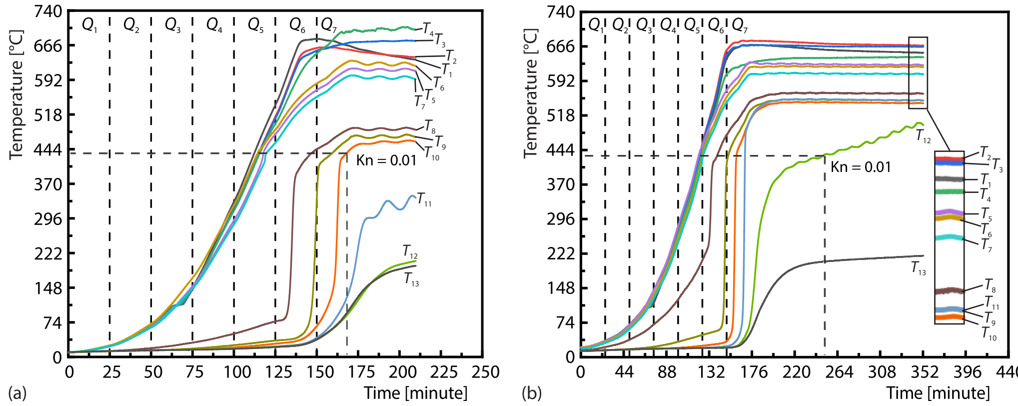

Figure 7. Startup curve of SHP; (a) when the length of ES is 1200 mm and (b) when the length of ES is 1225 mm

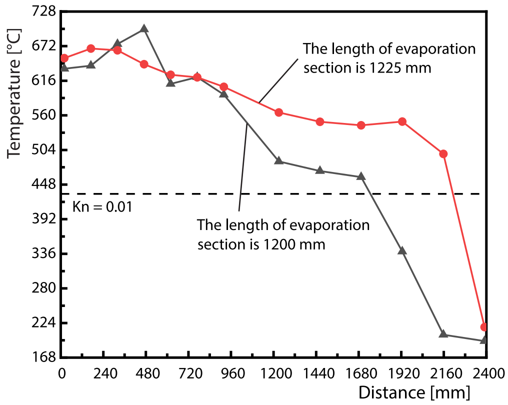

Figure 8. Axial temperature distribution of SHP under different ES lengths at steady-state

As the flow of sodium steam to the CS increases, the pressure difference within the SHP also increases. This occurrence results in the advancement of the temperature front towards the upper portion of the CS. Therefore, when the length of the ES of the SHP is 1225 mm, the CS's wall temperature of the SHP increases significantly. This phenomenon can also be seen in fig. 8.

In addition, the thermal resistance of the SHP under the aformentioned two working conditions is calculated by eq. (1). It is found tha when the length of the ES of the SHP increases from 1200 mm to 1225 mm, the thermal resistance decreases from 0.086-0.046 °C/W. In conclusion, increasing the length of the ES of the SHP cannot only significantly promote the start-up of the SHP, but also improve the startup performance of the SHP. This result is the same as that obtained in the literature [22].

Numerical model

To further investigate the heat transfer characteristics of SHP with a large aspect ratio, a numerical calculation model is developed and experimentally validated in this study. Since this paper mainly discusses the heat transfer of HTSHP under semi-steady-state, the freezing start, *i.e.* the melting of liquid metal sodium at the initial stage, is not considered.

Physical model

The simulation in this study utilizes a 2-D calculation model, depicted in fig. 9. The geometric dimensions of the model are the same as those of the components used in the experimental device. Before numerical calculation, the following assumptions are made for the model:
- The vapor is considered to be saturated at $t = 0$.
- The flow in the steam zone is considered as laminar flow.
- The solid skeleton of fluid and porous media is of constant physical properties.
- Porous media are homogeneous isotropic media filled with fluid.
- Thermal dispersion effect of porous media is neglected.
- The local heat balance is observed between porous media and fluid.

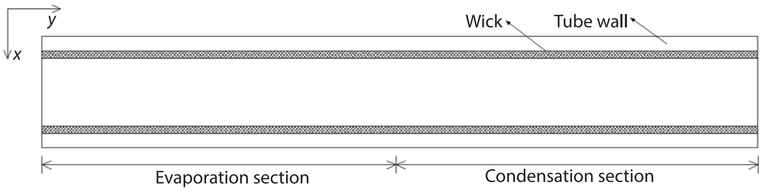

Figure 9. Calculation model of SHP

Governing equations

Continuity equation:

$$\frac{\partial \alpha_{\mathrm{v}}}{\partial t} + \nabla\left(\vec{\mathrm{v}}\alpha_{\mathrm{v}}\right) = \frac{S_{\mathrm{v}}}{\rho_{\mathrm{v}}} \tag{6}$$

$$\frac{\partial \alpha_{l}}{\partial t} + \nabla\left(\vec{\mathrm{v}}\alpha_{l}\right) = \frac{S_{l}}{\rho_{l}} \tag{7}$$

where t is the time, $\vec{\mathrm{v}}$ – the velocity in the Y-direction, and S – the source term produced by phase transition.

Momentum equation:

$$\frac{\partial\left(\rho_m \vec{\mathrm{v}}\right)}{\partial t} + \nabla\left(\rho_m \vec{\mathrm{v}}\vec{\mathrm{v}}\right) = -\nabla p + \nabla\left[\mu_{m,\mathrm{eff}}\left(\nabla\vec{\mathrm{v}} + \left(\nabla\vec{\mathrm{v}}\right)^T\right)\right] + \rho_m \vec{\mathrm{g}} + \vec{\mathrm{F}}_\sigma \tag{8}$$

where ρ, p, $\vec{\mathrm{g}}$, $\vec{\mathrm{F}}_\sigma$ are the fluid density, fluid pressure, gravitational acceleration, and steam water surface tension, respectively.

In porous media, the local heat balance is observed between porous media and fluid, and the energy equation is:

$$\frac{\partial}{\partial t}\left[\varepsilon\rho H + \left(1-\varepsilon\right)\rho_g H_g\right] + \nabla\left[\vec{\mathrm{U}}\left(\rho H + p\right)\right] = \nabla\left(kT\right) + S_h \tag{9}$$

where $\vec{\mathrm{U}}$ is the velocity vector, p – pressure, ε – the porosity of the porous medium, S_h – the energy source term.

Boundary conditions

The wall temperature obtained in section *Results and discussion* for the 1225 mm ES length is fitted with the axial distance, and the eqs. (10) and (11) are obtained, which are used as the boundary conditions of the ES and the CS, respectively in this simulation:

$$T_\mathrm{e} = -853.85y^4 + 1907.8y^3 - 1435.7y^2 + 321.6y + 926.05 \ \text{(Evaporator)} \tag{10}$$

$$T_\mathrm{c} = -2602.5y^4 + 13712y^3 - 33680y^2 + 36184y - 13510 \ \text{(Condenser)} \tag{11}$$

Considering the minimal heat loss at both ends of the SHP, it is assumed that the ends are insulated and non-slip:

$$\frac{\partial T}{\partial y} = 0 \ \text{ at } \ y = 0 \ \text{ and } \ y = 2400 \tag{12}$$

$$v = 0 \ \text{ at } \ y = 0 \ \text{ and } \ y = 2400 \tag{13}$$

Because the boiling point of sodium metal is 1154.55 K, in order to save calculation time, the initial temperature of the model is set to 1073.15 K. The finite volume method is employed to discretize the control equation, while the momentum and energy equations adopt the second-order upwind scheme. The pressure equation adopts the PRESTO discrete scheme, and the velocity and pressure coupling adopt the SIMPLE algorithm.

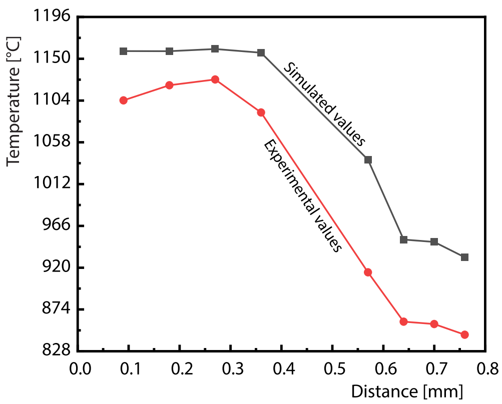

Figure 10. Comparison between experimental and simulated values of surface temperature of SHP

Numerical simulation results

Model validation

The SHP described in reference [23] is utilized for numerical simulation validate the accuracy of the aforementioned calculation model. According to the test conditions in [23], the constant heat flow boundary condition is taken for the ES during the simulation, q_e= 46536.5 W/m^2. The third boundary condition is taken for the CS, h = 180 W/m^{2}K, T_air = 293.15 K. Adiabatic wall boundary conditions are assumed. The chart presents both the simulation results obtained in this study and the experimental results documented in [23]. As shown in fig. 10, The calculated results exhibit a satisfactory agreement with the experimental data, with a maximum relative error of 13.5%.

Velocity distribution

Figure 11 depicts the axial distribution curve of velocity for steam and liquid phases. Due to the uneven evaporation of working medium in the ES and condensation in the CS, the axial velocity of steam exhibits large fluctuations, as shown in fig. 11(a). At a distance of 1.43 m from the end of the ES, the axial velocity of the gas in the steam chamber of the SHP reaches its maximum value of 4.48 m/s. The axial velocity of liquid reaches the maximum value of 1.51 m/s at 0.606 m from the end of ES, as shown in fig. 11(b).

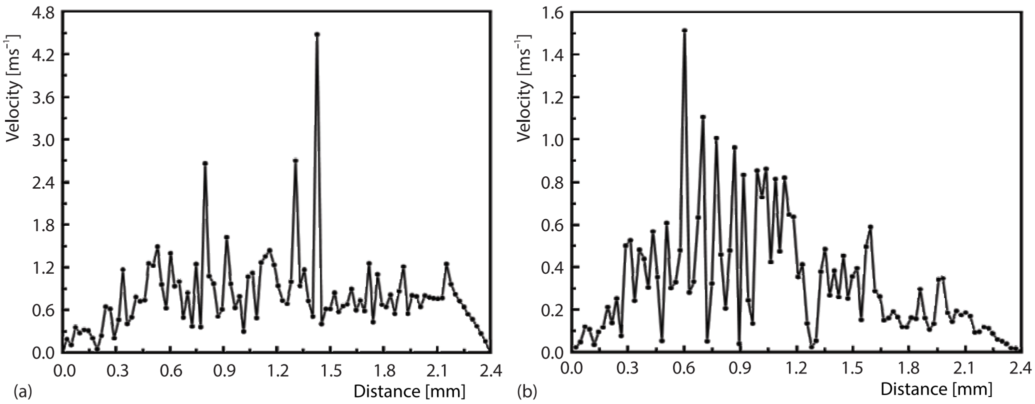

Figure 11. Longitudinal velocity distribution: (a) vapor and (b) liquid

Pressure distribution

Figure 12 presents the axial distribution curve of pressure for both the liquid and steam phases. As shown in fig. 12, with the increase of axial distance, the axial pressure of liquid and steam in the SHP shows a downward trend. However, the difference is that the axial pressure of steam only decreases from –0.015 kPa to –14.24 kPa, while the axial pressure of liquid decreases from $1.71 \cdot 10^{-6}$ kPa to –737.9 kPa, the axial pressure drop of liquid is significantly greater than that of steam.

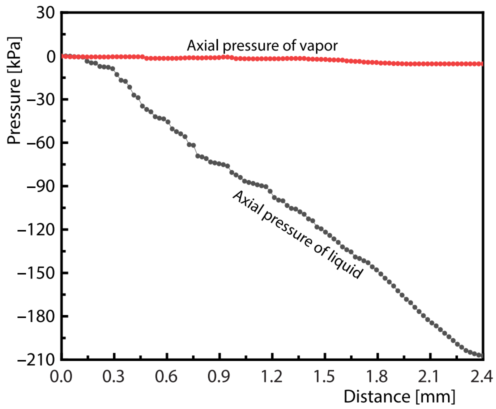

Figure 12. Axial pressure distribution of liquid and steam

It is evident that the pressure drop in the SHP's two-phase flow is predominantly governed by the liquid phase pressure drop. The small axial pressure drop of steam in the SHP shows that the SHP has good isothermal performance. The liquid-flow in the wick experiences a significant pressure drop from the CS to the ES along the axial direction, suggesting that the capillary pressure supplied by the wick primarily acts to overcome the resistance of liquid-flow within the wick.

Conclusions

In this paper, a HTSHP with a length-diameter ratio of 126 was designed, and its start-up characteristics were experimentally studied. The wall temperature changes of SHP under fixed power heating and variable power heating were compared. The impact of varying ES lengths on the onset of freezing in a sodium heat pipe was examined and discussed. The findings indicate that the temperature distribution within the ES is more uniform when employing the variable power heating mode. At the same time, the temperature at the top of the CS is higher than that under the fixed power heating mode. The increase of ES length not only significantly increases the maximum temperature of CS, but also effectively improves the starting performance of SHP. The length-to-diameter ratio has a significant impact on the start-up of the SHP.

The FLUENT software was utilized to simulate and validate the two-phase flow of the working fluid in the designed SHP. It was discovered that the maximum error between the numerical calculation results and the experimental results was 13.5%. The model can be employed for future performance prediction and theoretical investigations of similar heat pipes.

Nomenclature

D – diameter, [mm]
Kn – Knudsen number
L – length, [mm]
Q – heat transfer rate, [W]
R – thermal resistance, [°CW^{-1}]
P – pressure, [Nm^{-2}]
T – temperature, [°C]

Acronyms

CS – condensation section
ES – evaporation section
ENHS – encapsulated nuclear heat source
HP – heat pipe
HTSHP – high temperature sodium heat pipe
SHP – sodium heat pipe

Greek symbols

δ – thickness, mm
κ – Boltzmann constant, [JK^{-1}]
λ – Molecular mean free path, [m]
σ – effective molecular diameter, [m]

Subscripts

e – evaporator
c – condenser
in – input
sat – saturation
sys – system
v – vapor phase

References

[1] Poston, D. I., Nuclear Design of the SAFE-400 Space Fission Reactor, *Proceeding*s, Int. Congress on Advanced Nuclear Power Plants (ICAPP), Hollyvood, Fla., USA, 2002
[2] Greenspan, E., *et al*., The Long-Life Core Encapsulated Nuclear Heat Source (ENHS) Generation IV Reactor, *Proceedings*, Int. Congress on Advanced Nuclear Power Plants (ICAPP), Budapest, Hungary, 2002
[3] Greenspan, E., Solid-Core Heat-Pipe Nuclear Battery Type Reactor, tech. Report, Research Proposal Submitted for the DOE Nuclear Engineering Education Research (NEER) Program, US Depa of Energy, Ouk Ridge, Tenn., USA, 2005
[4] Faghri, A., Review and Advances in Heat Pipe Science and Technology, *Jou. Heat Transfer*, *134* (2012) 12, 123001
[5] Ma, T., *et al*., 2016. Frozen Start-Up Performance of a High Temperature Special Shaped Heat Pipe Suitable for Solar Thermochemical Reactors, *Appl. Therm. Eng*., *109* (2016), Part A, pp. 591-599
[6] Zhang, H. Z., *et al*., 2021. Sodium-Potassium Alloy Heat Pipe Under Geyser Boiling Experimental Study: Heat Transfer Analysis, *Energies*, *14* (2021), 22, 7582
[7] Jang, J. H., 1995. Startup Characteristics of a Potassium Heat Pipe From the Frozen State, *Jou. Thermophysics Heat Transfer*, *9* (1995), 1, pp. 117-122
[8] Chen, H. X., *et al.*, Experimental study on Frozen Startup and Heat Transfer Characteristics of a Cesium Heat Pipe under Horizontal State, *Int. J. Heat Mass Transfer*, *183* (2022), 122105
[9] Toumier, J. M., El-Genk, M. S., A Vapor Flow Model for Analysis of Liquid-metal Heat Pipe Startup from a Frozen State, *Int. J. Heat Mass Transfer*, *39* (1996), 18, pp. 3767-3780
[10] Ge, P. H., *et al*., Numerical Simulation of Start-Up Characteristics of High Temperature Heat Pipe Based on SIMPLEC Algorithm, *Atomic Energy Science and Technology*, *51* (2017), 11. pp. 1974-1981
[11] Ma, Y. G., *et al*., Effect of Inclination Angle on the Startup of a Frozen Sodium Heat Pipe, *Appl. Therm. Eng*., *201* (2022), 117625
[12] Wang, C. L., *et al*., Experimental Study on Startup Performance of High Temperature Potassium Heat Pipe at Different Inclination Angles and Input Powers or Nuclear Reactor Application, *Ann. Nucl. Energy*, *136* (2020), 107051
[13] Yang, L., *et al*., Experimental Investigate on Thermal Properties of a Novel High Temperature Flat Heat Pipe Receiver in Solar Power Tower Plant, *Appl. Therm. Eng*. *109* (2016), Part A, pp. 610-618
[14] Yu, P., *et al*., Restart Characteristics of High-Temperature Sodium Heat Pipe, *Proceedings of the CSEE*, *35* (2015), 2, pp. 404-410
[15] Guo, Q., *et al*., Influence of Inclination Angle on the Start-up Performance of a Sodium-Potassium Alloy Heat Pipe, *Heat Transfer Eng*., *39* (2018), 17-16, pp. 1627-1635

[16] Ding, L., *et al*., Starting Performance of High Temperature Heat Pipe in Solar Receiver, *Jou. Nanjing Tech University: Nat. Sci. Ed*., *31* (2009), 05, pp. 79-85
[17] Yu, Q. Y., *et al*., Study on Characteristics of High Temperature Heat Pipe Based on CFD Method, Nuclear Power Engineering, *43* (2022), 02, pp. 70-76
[18] Ji, Y. L., *et al.*, An Experimental Investigation on the Heat Transfer Performance of a Liquid Metal High-Temperature Oscillating Heat Pipe, *Int. J. Heat Mass Transfer*, *149* (2020), 119198
[19] Cao, Y., Faghri, A., A Numerical Analysis of High-Temperature Heat Pipe Startup from the Frozen State, *Jou. Heat Transfer*, *115* (1993), 1, pp. 247-254
[20] Qian, Z. Y., *Thermal Properties of Low Melting Point Metals*, Science Press, Beijing, China, 1989, pp. 514-515
[21] Zhang, M. H., *et al*., Effect of Non-Condensable Gas on Heat Transfer Characteristics of High Temperature lithium Heat Pipe, *Atmoic Energy Sci. Techno.*, *56* (2022), 06, pp. 1094-1103
[22] Zhao, W. L., *et al*., Effect of Evaporation Section Length and Liquid Filling Capacity on Start-Up Process of High Temperature Sodium Heat Pipe, *Chemical machinery*, *30* (2022), 05, pp. 259-262
[23] Teng, W. F., *et al*., Experimental Investigations on Start-Up and Thermal Performance of Sodium Heat Pipe under Swing Conditions, *Int. J. Heat Mass Transfer*, *152* (2020), 119505

Paper submitted: October 30, 2023
Paper revised: January 2, 2024
Paper accepted: January 9, 2024